A hybrid approach for dynamic instability analysis of single-layer latticed domes with uncertainties

Ning An[1,2], Huidong Zhang[1,2 *], Xinqun Zhu[3], and Fei Xu[1,2]

[1]School of Civil Engineering, Tianjin Chengjian University, Tianjin 300384, China

[2]Tianjin Key Laboratory of Civil Buildings Protection and Reinforcement, Tianjin 300384, China

[3]School of Civil and Environmental Engineering, University of Technology Sydney, NSW 2007, Australia

Abstract: Currently there is no unified criterion to evaluate the failure of single-layer latticed domes, and an accurate numerical model is usually needed for the nonlinear time-history analysis (NTHA), which the uncertainties in practical engineering structures are not considered. The seismic instability of domes subjected to earthquake ground motions has not been widely investigated. In this paper, a new approach is developed to automatedly capture the instability points in the incremental dynamic analysis (IDA) of single-layer lattice domes by integrating different efficient and robust methods. Firstly, the seismic fragility analysis with the instability parameters is carried out using the bootstrap calibration method for the perfect domes. Secondly, based on the Sobol sequence, the Quasi-Monte Carlo (QMC) sampling method is used to calculate the failure probability of the domes with uncertain parameters efficiently, in which the truncated distributions of random parameters are considered. Thirdly, the maximum entropy principle (MEP) method is used to improve the computational efficiency in the analyses of structures with uncertainties. Finally, the uncertain interval of the domes is determined based on the IDA method. This proposed method has been used to investigate the instability of single-layer lattice domes with uncertain parameters. The results show that the proposed approach could determine the probability of structural failure with the high efficiency and reliability. The limitations of the approach for the parallel computation are also discussed.

Keywords: Single-layer lattice dome; Dynamic instability; Failure probability; Quasi-Monte Carlo; High efficiency

1. Introduction

The single-layer latticed dome is widely used because of its large size and light weight. However, its dynamic demands are highly nonlinear because its structural resistance capacity is affected by many factors,[1] including various uncertainty sources in engineering construction. In deterministic methods, these sources are ignored in structural modelling. However, considering uncertain sources is necessary for the reliability of analysis results. Usually, probabilistic structural analysis methods are used in modelling structures with uncertainties. To reduce the computing time, high-precision sampling methods are also necessary, especially in nonlinear dynamic time-history response analyses (NDTHRA).

For modelling a practical structure, uncertain sources can be classified into two categories: the uncertainty of the assumed external excitations, such as the uncertain number of selected earthquake ground motions, and the uncertain parameters in the numerical model.[2] The number of selected ground motions is an important uncertain factor in estimating mean structural demands because the trade-off between variance and bias of seismic demands is affected by the number of selected ground motions. For model parameters, the important uncertain sources mainly include (1) the constitutive models of the material, (2) the damping mechanism, (3) the various geometry imperfections, and (4) the internal structural load.

In constitutive models of materials, the elastic modulus and material strength are closely related to structural instability;[3] nevertheless, the elastic modulus and material strength vary obviously in engineering structures. In the damping mechanism, different damping mechanisms exist in single-layer

*Correspondence to: Huidong Zhang, School of Civil Engineering, Tianjin Chengjian University, China

E-mail: zhhuidong@126.com

latticed domes, which leads to the uncertainty of the evaluation of serviceability limit states.[4] In deterministic numerical modelling, it is often assumed that the model has no initial imperfections, but this is not true in practice. The mechanical behaviours of steel domes are substantially affected by imperfections;[5, 6] therefore, they are imperfection-insensitive,[7] in which random nodal deviations have a substantial influence on the stability of domes.[8] In addition, the internal structure load is also a key factor, whose variation has an important effect on the seismic response of domes.[9] In previous studies, each uncertain variable is considered to have a specific unbounded probability distribution, but in fact, the bounds of each variable exist.[10] Therefore, the variables need to be truncated in the specific unbounded probability distributions.

The performance assessment of a structure is usually described in terms of demands and capabilities, and the capability refers to the maximum acceptable structural response. The incremental dynamic analysis (IDA) method can be used to calculate the seismic demands and capacities and is widely used in nonlinear dynamic analyses.[11] Originally, IDA was applied to the analyses of concrete structures and later applied to other structural systems.[12] In IDA, to obtain the dynamic demands under different earthquake intensity levels, the constant loading step for the scale factors of the acceleration values is used because of its convenience. Based on an IDA curve, the intensity level of the ground motion and the structural demand can be described by an intensity measure (IM) and an engineering demand parameter (EDP).[13] The maximum demands for a single-layer latticed dome have been investigated using IDA.[14] With the benefit of IDA, seismic fragility analysis can be performed to quantify the failure probability of a given instability level using a function with the independent variable IM.[15] However, the accuracy of this fragility function depends on the sample characteristics and sample size. To solve this problem, the bootstrap method is used to improve the sample characteristics in a small sample size. Some researchers [16-18] have carried out engineering applications using the bootstrap method with small sample sizes. This method is widely used in management science, risk analysis, and clinical trials fields,[19] and it has not been widely applied in the analyses of civil structures. In this paper, this method is used in structural analyses because of its advantages in statistics.

When carrying out the analyses of structures with uncertainties, it is noted that an appropriate sampling method is important for structural analyses. Among the probabilistic models for uncertainty propagation, the Monte Carlo (MC), quasi-Monte Carlo (QMC), and Latin hypercube sampling (LHS) methods are widely used due to their general applicability and robustness, and they are the most reliable methods for calculating the probability of failure.[20] For the direct MC method, its rate of convergence $O(1/\sqrt{n})$ is very slow,[21] while the quasi-Monte Carlo (QMC) method has a smaller error convergence order, which is asymptotically equal to $O(1/n)$.[22] Compared with the direct MC method, it is evident[23] that the QMC method based on the Sobol sequence is a better method, and the results are consistent with the theoretical predictions. In this paper, Sobol' sequence is adopted to perform the QMC simulations. Moreover, the maximum entropy principle (MEP) is a statistical tool that predicts the most unbiased probability distribution from samples.[24] According to the probability distributions of variables, it is easy to obtain the probability of structural failure; thus, the MEP can further reduce the sample size when capturing the probability of failure. In this paper, the MEP is introduced to calculate the probability of failure.

In the framework of this paper, first, the perfect single-layer latticed dome is investigated using the deterministic method to find the instability points under 7 typical earthquake ground motions based on IDA, and the displacement characteristics of the dome structure are analysed. The seismic fragility analysis of the perfect structure is carried out to describe the probability of structural failure, and two

methods for solving the probability of structural failure are discussed. Then, the single-layer latticed dome with uncertain parameters is investigated using the structural probabilistic methods, in which the QMC and the MEP methods are utilized to evaluate the probability of failure, and the efficiency of the sampling methods are also compared, including the MC, the QMC, and the LHS methods. Finally, the advantages and disadvantages of the used, improved, and proposed methods in this paper are discussed.

2. Methods based on IDA

2.1 IDA with a tracing algorithm

IDA curves can be described by the relationship between IM and EDP. The peak ground acceleration (PGA) is a common IM.[25] In this study, to find accurate instability points, the statistical maximum displacement of all the nodes of a dome (U_{max}) was selected as the EDP.

In terms of the structural instability, at present, there is no unified criterion for judging the instability point of domes, and empirical methods are usually considered.[1, 26] However, the literature[27] provided the general regulation on the global stability limit for welded steel-moment frame buildings: the straight line slope between consecutive points is less than 0.2 times the elastic slope. In this paper, the regulation of the global stability of the domes is introduced for the domes in the absence of a better judgement criterion as a reference. Researchers have developed algorithms to determine the instability point. The stepping algorithm is a common method to increase the IM until the structure loses stability. Although this method is simple and direct, the quality of the IDA curve depends on the size of the step. If the step size is too large, it is difficult to capture the exact location of structural instability; if the step size is too small, the calculations are time-consuming. Another method is the hunt & fill tracing algorithm,[28] which can overcome these difficulties by changing its steps automatically. In this paper, a new interpolation algorithm is considered to improve the hunt & fill tracing algorithm to accurately calculate the incremental dynamic curve and find the instability point.

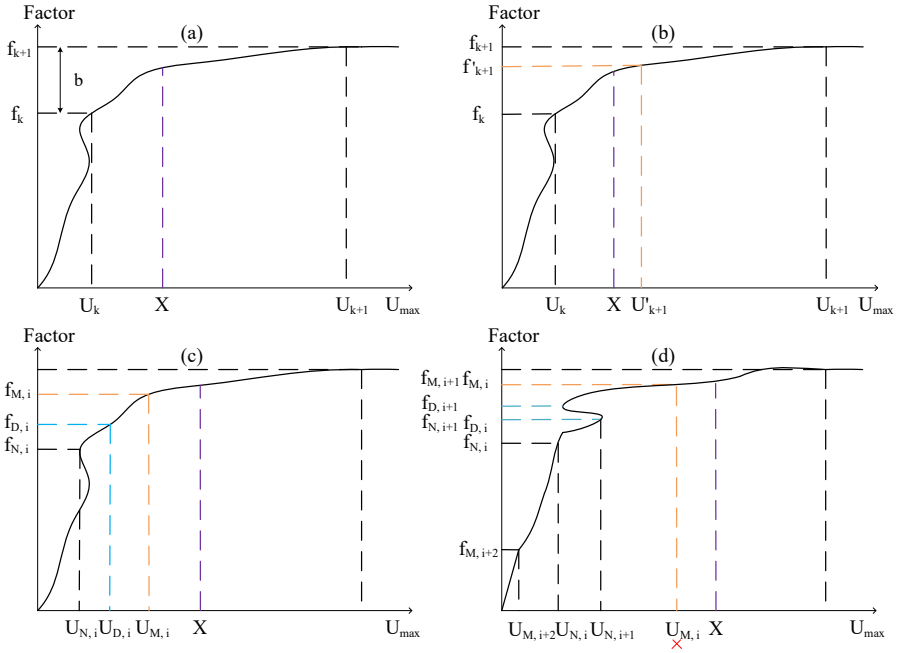

Fig. 1. The tracing algorithm of IDA.

The interpolation algorithm used in this paper is described in **Fig. 1**. The factor f_{k+1} increases by a constant b based on the factor f_k of the k^{th} step, that is, $f_{k+1} = f_k + b$, as shown in **Fig. 1(a)**. If the use of the factor f_{k+1} results in U_{max} exceeding a specified large value X, the constant b is reduced, as shown in **Fig. 1(b)**. The factor of the $(k+1)^{th}$ step is changed to $f'_{k+1} = f_{k+1} - (f_{k+1} - f_k)/3$

until U_{max} is less than X. Next, the factors corresponding to the displacement interval within the range of (0, U'_{k+1}) are interpolated. The interpolated factor is $f_{D,i} = f_{N,i} + (f_{M,i} - f_{N,i})/3$, in which $f_{M,i}$ and $f_{N,i}$ are the large and small factors corresponding to the displacement interval, respectively, as shown in **Fig. 1(c)**. Here, to ensure the calculation accuracy, the number of calculations is set to T times. In this paper, the effect of the calculation times T on the accuracy is discussed. In addition, in the above calculation process, if $f_{M,i}$ and $f_{M,i+1}$ are the same, $U_{N,i+2}$ and $U_{M,i+2}$ are chosen, which are less than $U_{M,i}$, as shown in **Fig. 1(d)**. This can reduce the unnecessary calculations that are introduced when the displacement is too large.

The above algorithm avoids the disadvantages of the traditional constant step algorithm and saves calculation time because of its characteristic of automatically calculating the magnification factor. Therefore, the computing efficiency and accuracy can be greatly improved. A comparison between the two algorithms is discussed in this paper.

2.2 Fragility analysis

Generally, the fragility function can be expressed in the following form:[29]

$$P_f[D > C|IM = im] = 1 - \Phi\left[\frac{\ln\mu_C - \ln\mu_D}{\sqrt{\sigma^2_{\ln D} + \sigma^2_{\ln C}}}\right] \quad (1)$$

in which D is the seismic demand; C is the structural capacity, which is assumed to be lognormally distributed;[30] μ_C is the median value of the structural capacity; μ_D is the median value of the seismic demand; and $\sigma_{\ln D}$ and $\sigma_{\ln C}$ are the associated logarithmic standard deviations of the demand and capacity, respectively.

In this paper, the second order polynomial was used to fit the data to obtain better fitting effectiveness:

$$\ln\mu_D = \alpha_0 + \alpha_1 \ln IM + \alpha_2 (\ln IM)^2 \quad (2)$$

in which α_0, α_1, and α_2 are the coefficients that can be obtained by regression analyses. $\sigma_{\ln D}$ can be calculated by the following equation:[29]

$$\sigma_{\ln D} \approx \sqrt{\frac{\sum_{i=1}^{N} (\ln D_i - \ln\mu_D)^2}{N-2}} \quad (3)$$

in which D_i is the data from the IDA curves, and N is the size of the data points. In this paper, μ_C and $\sigma_{\ln C}$ are the mean value and the standard deviation of the displacements of the instability points, respectively. After the IDAs were performed using the deterministic method, these results were used for regression analyses.

Fragility analysis is a classical method, but its accuracy greatly depends on the size of the earthquake motion records. Considering the trade-off between bias and variance and calculation time, the number of ground motion records used in structural analyses is usually limited. Therefore, in this paper, the bootstrap resampling method is introduced to increase the sample size and improve the estimation accuracy of the statistical parameters; see the following section.

2.3 Bootstrap calibration for the statistical parameters

The bootstrap method is illustrated in **Fig. 2**. A new sample set x^* with a sample size n is extracted and generated from the original data set x with a sample size n using the equal probability method. It should be noted that some data in the new set x may be the same. The resampling process is carried out B times. Usually, the resampling time of B=200 is sufficient for estimating standard errors in the bootstrap method.[31] From the new sample set x^*, the statistical parameter $\hat{\theta}^*(i)$ can be computed, which can be the mean value, the standard deviation, or the variance. Finally, the mean value and

variance of the statistical parameters $\hat{\theta}^*(i)$ can be obtained. This process is able to calibrate the initial data set x.

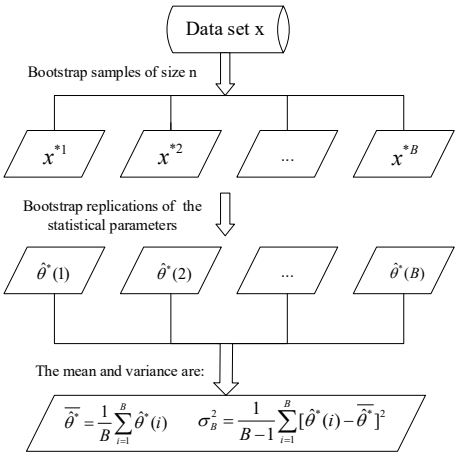

Fig. 2. Flowchart of the bootstrap method

In this process, a larger number of resampling times B can obtain better accuracy. In this paper, the resampling time B is set to =10^4. A simple example is given to describe the accuracy of the method in evaluating the standard deviation of the parameters assuming that X is a random variable with a normal distribution, $X_v \sim N(1, 0.5^2)$. The standard deviations using the bootstrap method and the LHS method are listed in **Table 1** under different small sampling sizes. The theoretical value of the standard deviation of X_v is $\sigma = 0.5$. From **Table 1**, it seems that the standard deviations estimated by the bootstrap method are the same as those estimated by LHS under small sampling sizes.

Table 1 Standard deviation σ with small sample sizes.

Sample size	σ_e (bootstrap method)	σ_e (LHS method)
7	0.3730	0.4209
20	0.4937	0.5097
30	0.4921	0.5058
40	0.5058	0.5164
60	0.5057	0.5124
100	0.5009	0.5031

Table 2 Accumulative errors of the two methods.

Sample size	error, e (bootstrap method)	error, e (LHS method)
7	2.4681	2.9326
20	0.9018	0.9989
30	0.6321	0.7037
40	0.4701	0.5147
60	0.3329	0.3601
100	0.2237	0.2298

However, the randomness of resampling has an effect on the statistical value. Therefore, to further evaluate the precision of the two methods, each sample process in **Table 1** is replicated 1000 times. The evaluation formula of the accumulative error is as follows:

$$e = \sqrt{\sum_{m=1}^{1000}(k - 0.5)^2} \tag{4}$$

in which $k = \sigma_e$. The accumulative errors are listed in

Sample size	σ_e (bootstrap method)	σ_e (LHS method)

7	0.3730	0.4209
20	0.4937	0.5097
30	0.4921	0.5058
40	0.5058	0.5164
60	0.5057	0.5124
100	0.5009	0.5031

Table 2. It can be seen that the accumulative error using the bootstrap method was smaller than that using the LHS method for each sample process, indicating that compared with the LHS method, the bootstrap method has a higher precision in estimating statistical parameters in a small sample size.

3. Sampling methods

3.1 Sobol sequence sampling

In the QMC method, the Sobol sequence is used for sampling because of its uniformity and ease of construction. In the 1-dimensional case, the primitive polynomial that has the degree s and coefficients a_i (between 0 and 1) can be written as:

$$p(x) = x^s + a_1 x^{s-1} + \cdots + a_{s-1} x + 1 \tag{5}$$

The detailed construction of $p(x)$ can be found in.[32] These coefficients of the primitive polynomial can define a sequence of odd integers with the following recursive relation:

$$m_k = 2a_1 m_{k-1} \oplus 2^2 a_2 m_{k-2} \oplus \cdots \oplus 2^{s-1} a_{s-1} m_{k-s+1} \oplus 2^s m_{k-s} \oplus m_{k-s} \tag{6}$$

in which $\oplus$ is the bit-by-bit exclusive-or operation, and m_k is less than 2^k; here, $k = 1,2,\ldots,s$. The direction number is defined as:

$$v_k = \frac{m_k}{2^k} \tag{7}$$

The Sobol points can be recursively generated by the following equation:[33]

$$x_{k+1} = x_k \oplus v_{c_k} \tag{8}$$

in which the symbol c_k represents the index of the rightmost zero bit in the binary representation of the integrate k. The literature[33, 34] provides more details for creating the Sobol sequence.

However, the QMC method still requires a large number of calculations to obtain the probability of failure. To reduce the computing number, the MEP is used in this paper, as shown in the following section.

3.2 Maximum entropy principle

The MEP can obtain the probability density function (PDF) $f(x)$ of the estimated demand (such as the displacement) by maximizing the entropy, $H(X)$. The PDF can be solved by the following expressions:[24]

$$\begin{cases} \max\ H(X) = -\int f(x)\ln f(x)dx \\ s.t. \begin{cases} \int f(x)dx = 1 \\ \int x^i f(x)dx = b_i, \quad i = 1,\ldots,m \end{cases} \\ b_i = \frac{1}{N}\sum_{j=1}^{N} x^i \end{cases} \tag{9}$$

in which b_i is the origin moment of the i^{th} order, m is the highest order of the origin moment in the sample, and N is the sample size. Thus, $f(x)$ can be expressed as:[24]

$$f(x) = e^{-(\lambda_0 + \sum_{i=1}^{m} \lambda_i \mathrm{x}^i)} \tag{10}$$

in which λ_i denotes a Lagrange multiplier, and λ_0 is expressed as:

$$\lambda_0 = \ln\left(\int e^{-\sum_{i=1}^{m} \lambda_i \mathrm{x}^i} dx\right) \tag{11}$$

To solve λ_i with high efficiency, an unconstrained minimization method is used:[35]

$$\min \int e^{-\sum_{i=1}^{m} \lambda_i (\mathrm{x}^i - b_i)} dx \tag{12}$$

Thus, λ_0 and $f(x)$ can be solved by **Eqs. (11)**. In this paper, the above calculation was implemented by the genetic algorithm (GA).

4. Application

4.1 Dome structure

In this paper, the above proposed methods are applied to a single-layer latticed dome, which has a span of 60 m, a height of 12 m and a span-rise ratio of 5, as shown in **Fig. 3** and **Fig.** 4, respectively. The sizes of the tubular steel members used are listed in **Table 3**. The steel material properties of the members in the perfect dome are shown in **Table 4**. A load of 150 kg/m^2 was assumed, and the mass was concentrated at the joints. Both geometric nonlinearity and material nonlinearity were considered. The numerical analyses were carried out using the commercial FEM software ABAQUS. The source code of all the above algorithms is written in Python language. In the numerical model, each member was modelled with two beam elements with pipe cross sections.

In this paper, the structural reliability is evaluated by the failure probability of structures with uncertainties subjected to earthquake ground motions. The probability of failure P_f for structure instability is defined as:

$$P_f = P[y(x_1, x_2, \ldots x_n) - y^* \geq 0] \tag{13}$$

where x is the input variable, $y(x_1, x_2, \ldots x_n)$ is the corresponding structural response, and y^* is the structural instability point obtained based on the IDA of the perfect structure.

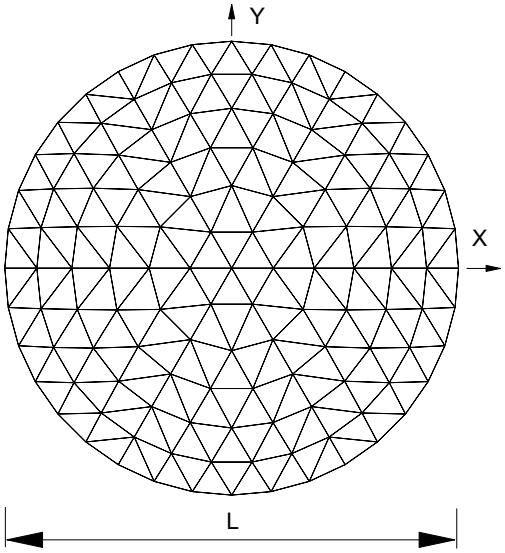

Fig. 3. Plane view of a dome.

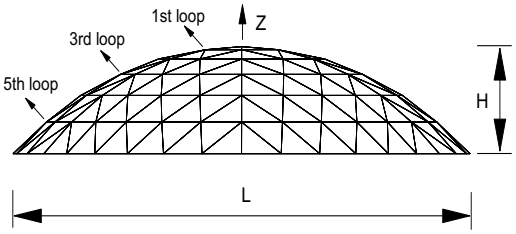

Fig. 4. Elevation view of a dome.

Table 3 Cross sections of the members.

Member	Size/mm
Ridge member	Φ=155; t=5.2
Hoop member	Φ=155; t=5.2
Diagonal member	Φ=148; t=5

Table 4 Material Properties.

Material parameters	Value
Elastic modulus /GPa	206
Yield strength, f_y /MPa	235
Ultimate strength, f_u /MPa	350
Ultimate strain	0.25

Poisson's ratio	0.3
Material density /(kg/m^3)	7800

4.2 Stochastic parameters

In this paper, the stochastic parameters considered include the node deviations, the load, the elastic modulus and yielding strength of the steel material, and the structural damping ratio, which are listed in **Table 5**. These stochastic parameters are collected from various sources[36-39] and are assumed to be independent. In practical engineering, the above variables have upper and lower bounds,[10] and they cannot be in the range of $(-\infty,+\infty)$. In this paper, the truncated distribution functions of the variables are used in structural analyses. The values are considered in the interval of $[\mu-2\sigma,\mu+2\sigma]$,[40] which can ensure that the probability that the variable values are within the range is 95.5% for variables with a normal distribution.

Table 5 Random parameters of the dome.

Name	Mean		COV	Distribution
	Reference[36-39]	In this paper		
Elastic modulus /GPa	206	206	0.03	Normal
Yield strength /MPa	251	235	0.081	Lognormal
Node deviation /m	L/500	0.12	0.5	Normal
Load /(kg/m^2)	143	150	0.1	Normal
Damping ratio	2%	2%	0.4	Normal

The nodal deviations are assumed to follow a normal distribution of $X\sim N(0,(R/2)^2)$,[8] in which R is the maximum nodal deviation, and it is set to 1/500 of the span.[41] In terms of damping in the dome, the conventional Rayleigh damping model is adopted for modelling structural damping in the dynamic structural analyses because of its convenience. The damping ratio in the k^{th} mode can be defined as:

$$\xi_k=\alpha\frac{1}{2\omega_k}+\beta\frac{\omega_k}{2} \tag{2}$$

For single-layer latticed domes subjected to earthquakes, a more appropriate damping model is recommended,[42] in which ω_i and ω_j are set as $0.667\omega_1$ and $3\omega_1$, respectively, and ω_1 is the first circle frequency. The parameters α and β can be obtained based on ω_i, ω_j and ξ_k. It should be noted that in structures with uncertainties, α and β are updated for each sample structure based on an eigenvalue analysis. Here, the structural damping ratio is set to 2%.[43]

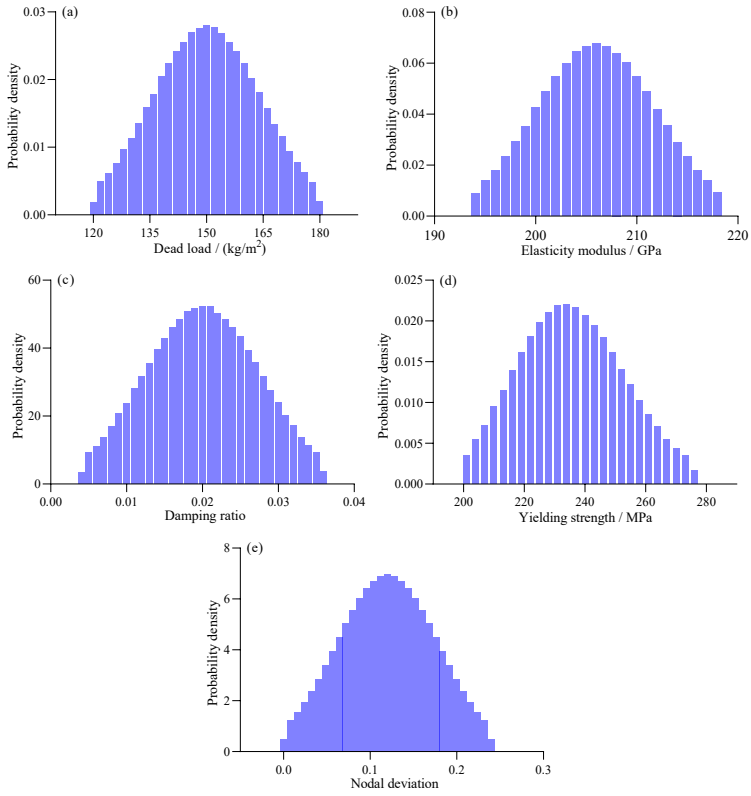

Fig. 5 Samples of the variables: (a) load, (b) elasticity modulus, (c) damping ratio, (d) yielding strength, and (e) single node deviation at the top.

At present, there is no unified criterion for the sample size of structures. Usually, the sample size is defined when the characteristics of the stochastic variables or the demand values of the structure tend to be stable. To speed up the computing process, a large number of sampling computing tasks can be completed in the parallel mode in Python by means of the multi-processing modules. The computer has 16 CPUs, one of which controls the main process that manipulates the script, and it does not participate in computing. Therefore, the calculation speed for the structures with uncertainties can be increased by 10-15 times for the QMC sampling method. In this paper, the sampling size in the sobol sequence was set to 9000. Based on this sampling size, the samples of the stochastic parameters are shown in **Fig.** . These samples effectively reflect the stochastic characteristics of the variables.

4.3 Earthquake ground motion

In this paper, three-dimensional earthquake ground motions are applied to the domes. Seven typical earthquake ground motion records are selected from the PEER Strong Ground Motion Database. The information of these records is listed in **Table 6**. The gravity load is applied first before the dynamic analyses, and then the seismic loads are applied to the domes.

Table 6 Seven typical earthquake ground motions.

Number	Earthquake	Year	Station name	PGA /(m/s^2)		
				x	y	z
1	Big Bear-01	1992	Silent Valley - Poppet Flat	0.589	0.680	0.461
2	Coyote Lake	1979	Gilroy Array #1	0.922	1.143	0.620
3	Duzce	1999	Lamont 531	1.211	1.572	0.622
4	Kobe	1995	Nishi-Akashi	4.736	4.550	3.789
5	Landers	1992	Twenty-nine Palms	0.786	0.591	0.388

6	Livermore-01	1980	Tracy - Sewage Treatment Plant	0.478	0.773	0.222
7	Morgan Hill	1984	Gilroy Array #1	0.682	0.968	0.924

4.4 A comparison between the constant step algorithm and the interpolation algorithm

Based on the above regulation on the global stability, the comparative results between the constant step algorithm and the interpolation algorithm in finding instability points are shown in **Fig.** under the Coyote Lake ground motion, in which IP represents the instability point. For the constant step algorithm, b is a constant (see Section 2.1), and T and T' are the required calculation times for finding the instability point.

According to **Fig. 6**, it can be seen that the instability point calculated using the constant step algorithm is not stable because when the step size is small, the instability point is easily disturbed by the negative slope, which makes the calculated instability displacement small (see the green point in **Fig. 6**). In addition, in the constant step algorithm, even if the step size is appropriate, the position of the instability point also fluctuates. In addition, the required calculation times T' in the constant algorithm have a substantial effect on the judgement of the instability point. Therefore, it is difficult to find the accurate position of instability points with a constant step algorithm. For the interpolation algorithm (current algorithm), it is observed that the instability points are stable. It is found that T in the interpolation algorithm has little effect on the judgement of the instability point. Therefore, the interpolation algorithm has more advantages than the constant step algorithm in finding the instability point of the dome.

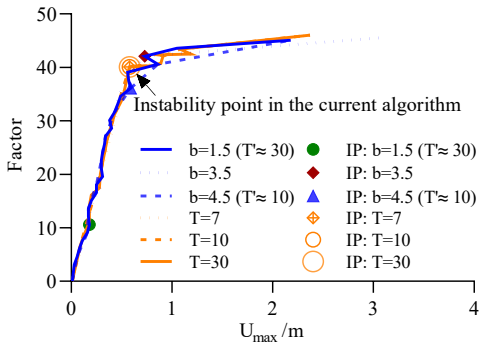

Fig. 6 IDA curve and instability point for different algorithms.

5. Results

5.1 IDA of the perfect structure

5.1.1 IDA curves

In the IDA, the maximum statistical displacement of the single node, U_{max}, is quantified using the following expression:

$$U_{max} = \max|_{i=1}^{i=n}(\max\left(\sqrt{U_{i,X,t}^2 + U_{i,Y,t}^2 + U_{i,Z,t}^2}\right)) \quad (3)$$

in which $U_{i,X,t}$, $U_{i,Y,t}$, and $U_{i,Z,t}$ are the displacement components in the X, Y, and Z directions at time t for the i^{th} node, respectively, and n is the number of nodes in the dome. The IDA curves and corresponding instability points of the dome structure under 7 earthquake ground motions are shown in **Fig. 5**. **Fig. 7** shows that the maximum PGAs of the earthquake ground motions range from approximately 10 m/s^2 to 50 m/s^2 when the dome loses stability. The mean curve of these IDA curves is constructed in **Fig. 7**, and it is found that the mean curve is close to the one under the earthquake Big Bear-01, and the corresponding instability point will be adopted to investigate the probability of failure of structures with uncertainties in the following sections.

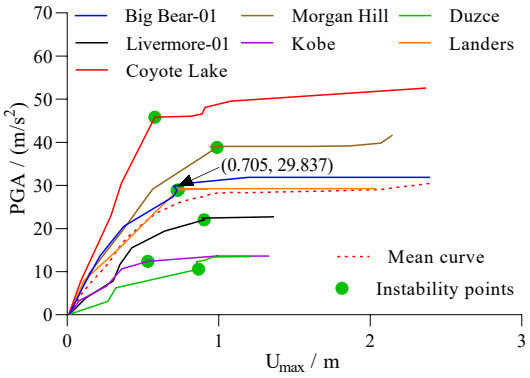

Fig. 5. IDA curves under different earthquakes.

5.1.2 Displacement characteristics in the IDA

5.1.2.1 Vertical displacement ratio

Compared with ordinary buildings, domes tend to lose instability in the vertical direction.[44] In this paper, this characteristic of the dome is quantified using the vertical displacement ratio (VDR), which is defined as:

$$VDR = \frac{|U_Z'|}{|U_X'|+|U_Y'|+|U_Z'|} \tag{4}$$

in which U_X', U_Y', and U_Z' are the three components of U_{max} in the X, Y, and Z directions, respectively.

The VDRs under different earthquakes are shown in **Fig. 6**. It is observed that the VDR presents a characteristic that decreases first and then increases as the PGAs increase, such as the blue dotted curve shown in the figure. After the dome loses stability, the VDRs increase sharply. In addition, almost all VDRs are larger than 0.5 under these earthquakes, indicating that the vertical displacement component plays an important role in the structural instability.

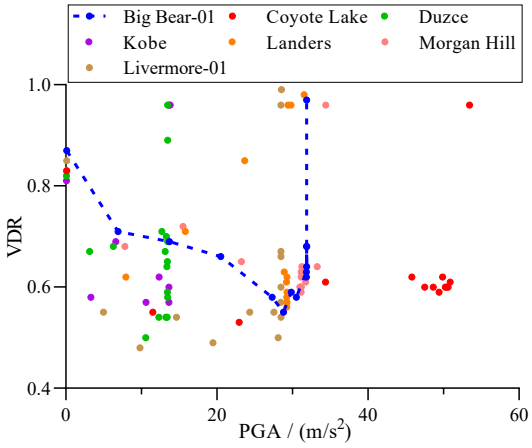

Fig. 6. Vertical displacement ratio (VDR) of the nodes under different earthquakes.

5.1.2.2 Maximum downward vertical displacement in the dome

According to the above analysis, $|U_Z'|$ has a substantial contribution to the maximum statistical displacement U_{max} because of the high VDRs. In this paper, the maximum downward vertical displacements ($U_{max,-Z}$) of the nodes in the direction of $-Z$ are further discussed under the earthquake Coyote Lake. A comparison between $|U_Z'|$ and $U_{max,-Z}$ is carried out in the process of IDA, and the node positions with the maximum displacements are also marked, as listed in **Table 7**, in which the smaller the node number, the closer the node position is to the top of the dome.

From **Table 7**, it is found that the values of $|U_Z'|$ and $U_{max,-Z}$ are almost identical, and the node positions with the maximum displacements are basically the same, except when the node numbers are 65 and 80. This indicates that $|U_Z'|$ or U_{max} can be directly replaced with $U_{max,-Z}$ to simplify the calculation investigating the characteristics of the structural instability of the dome, similar to the descriptions in the literature.[10] In addition, when the structure loses stability, it is found in the IDA process that the structural instability first originates from the local concavity at the nodes with the larger numbers, that is, the nodes that are close to the supports.

Table 7 A comparison between $|U_Z'|$ and $U_{max,-Z}$.

$\lvert U_Z' \rvert$ /m	Node No.	$U_{max,-Z}$ /m	Node No.
0.01	15	0.01	15
0.07	84	0.07	84
0.25	80	0.25	80
0.30	65	0.31	80
0.53	79	0.53	79
0.72	79	0.72	79
0.79	79	0.79	79
0.81	79	0.81	79
0.93	68	0.93	68
2.12	51	2.12	51
24.72	1	24.72	1

5.1.2.3 A parametric analysis for U_{max}

Usually, the structural displacement response depends on the design parameters. In this paper, the effects of the structural internal load and the span-depth ratio on U_{max} are further investigated under the earthquake Big Bear-01. **Fig. 7(a)** shows the effect of the structural load on U_{max}. It can be seen that the structural internal load has a very small effect on U_{max} when the PGAs are small; however, when the PGAs are large, the effect on U_{max} increases, and as expected, the greater the internal load, the greater U_{max} is. **Error! Reference source not found.** shows the effect of the span-depth ratio on U_{max}. The conclusion drawn from **Error! Reference source not found.** is consistent with that drawn from **Fig. 10(a)**.

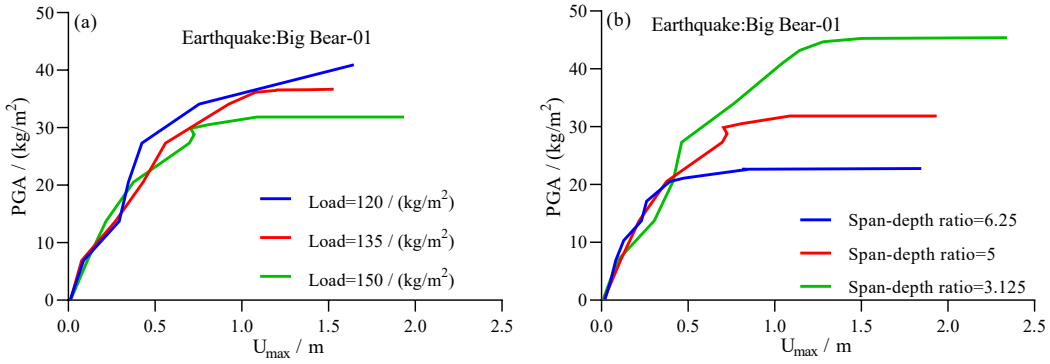

Fig. 7. The effect of the design parameters on U_{max}: (a) structural internal load, and (b) span-depth ratio.

5.2 Seismic fragility analysis for the perfect structure

The displacements at the instability points in **Fig. 7** are used for fragility analysis. The relationship between the EDP and the IM and its fitting curve are shown in Fig. 10. The fitting curve is used to carry out the fragility analysis. To increase the fitting precision of this curve, the fitting formula of the

quadratic polynomial is utilized.

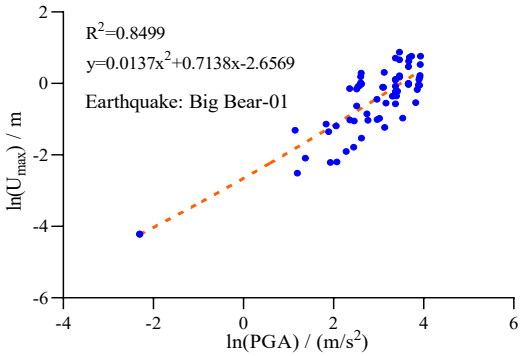

Fig. 8 Relationship between the EDP and the IM.

To construct the fragility curve, the statistical parameters are listed in **Table 8**. A comparison is carried out between the unmodified method and modified method. It is observed that the effect of the sample size on the precision of the parameters in the unmodified method is substantial, especially for the standard deviation, and a larger sample size can obtain a higher precision for the unmodified method.

Table 8 Statistical parameter estimation with the bootstrap method.

Statistical parameters	Unmodified value	Modified value, $\overline{\hat{\theta}^*}$
ln (μ_C)	-0.146	-0.146
$\sigma_{\ln C}$ (sample size=7)	0.137	0.127
$\sigma_{\ln D}$ (sample size=84)	0.518	0.518

According to the above two methods, two seismic fragility curves are shown in **Fig. 9**. In general, these two curves are similar, but when the PGA is small, the probability of instability using the unmodified method is higher than that using the modified method; when the PGA is large, the opposite is true. The probability of instability is slightly affected by the two methods.

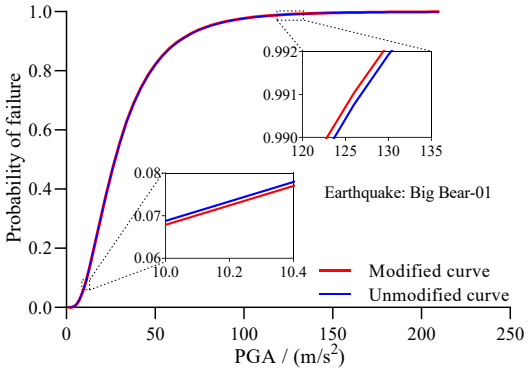

Fig. 9 The uncorrected and corrected seismic fragility curves.

5.3 Probability of dynamic instability of the structure with uncertainties

In this section, the probability of dynamic instability of the structure with uncertainties is investigated, and the earthquake Big Bear-01 is considered as the external excitation. According to the IDA for the perfect structure, 0.705 m is selected as the limit displacement (see **Fig. 7**). In this section, the calculation efficiency of different sampling methods is compared in terms of the probability of structural failure. The effect of the sample size on the dynamic demands and the errors of the probability of structural failure are also analysed.

5.3.1 Comparison of the sampling method efficiency

The scale factor of the earthquake ground motion Big Bear-01 is set to 30. The failure probabilities using different sampling methods for the structures with uncertainties are shown in Error! Reference

source not found.. It can be seen that the efficiency of LHS and QMC is relatively close, and the results converge for both methods when the sample number is close to 2800 in capturing the small probability of failure. However, for the direct MC method, the results converge when the sample number is close to 5000. Therefore, the calculation efficiency of the QMC and LHS methods in capturing the small probability of failure is higher than that of the MC. Although the LHS and QMC have similar calculation efficiencies, as an alternative, the QMC method that has not been widely investigated in the dynamic analyses of single-layer latticed domes is utilized for sampling. However, in estimating the mean structural dynamic demands, the mean value of U_{max} converges when the sample size is only close to 1000 because of the use of the truncation sampling method with the sobol sequence algorithm, as shown in **Fig. 13**.

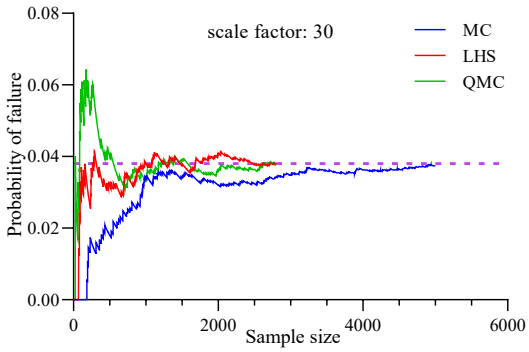

Fig. 10 Comparison of the sampling methods.

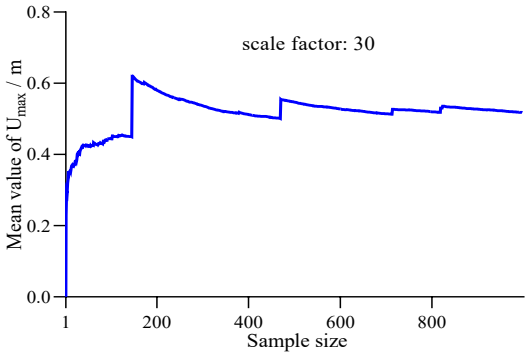

Fig. 11 Effect of the sample size on the dynamic demand.

In this study, the MEP is used to solve the probability density function of U_{max}. The first four order origin moments are used in the MEP method. A comparison is performed between the unmodified method and the modified method. The results are shown in **Fig. 14**.

Fig. 14(a) shows the results of the unmodified method. It is observed that for the unmodified method, it is difficult for the results to converge, especially for the 4^{th}-order origin moment; thus, the MEP method is time-consuming and unreliable for this application. To solve this problem, the modified MEP is proposed to improve the samples without changing the failure probability. The modified process is as follows: if $U_{max} > k$, then $U_{max} = k$ ($k > 0.705$ m); here, k is the cut-off point. The values of k are listed in **Table 9**. From **Table 9**, it can be seen that the probability of instability increases and then decreases with increasing k. Finally, the maximum value is selected as the result of the probability of structural failure.

Fig. 14(b) shows the results of the modified method. The results of the origin moment of each order converge when the sample sizes are only close to 500. Therefore, this method can obtain reliable calculation results. To further improve the precision, the number of samples is set to 2000 for the maximum entropy principle method.

Modified MEP	
The cut-off point k /m	Probability of failure
0.8	2.22%
0.9	3.37%
1.0	3.82%
1.1	3.77%
1.2	3.77%
1.3	3.77%
1.4	2.94%

1.5	2.62%

Table 10 lists the final results of the probability of structural failure and the error. From

Modified MEP	
The cut-off point k /m	Probability of failure
0.8	2.22%
0.9	3.37%
1.0	3.82%
1.1	3.77%
1.2	3.77%
1.3	3.77%
1.4	2.94%
1.5	2.62%

Table 10, compared with the QMC method, the probability of failure using the modified MEP method is less than that using the QMC method.

When the scale factors are 29 and 28, the final results of the probability of structural failure are listed in **Tables 11 and 12**, respectively. According to **Tables 10-12**, it is evident that with a decrease in the probability of failure, the error of estimating the probability of failure increases.

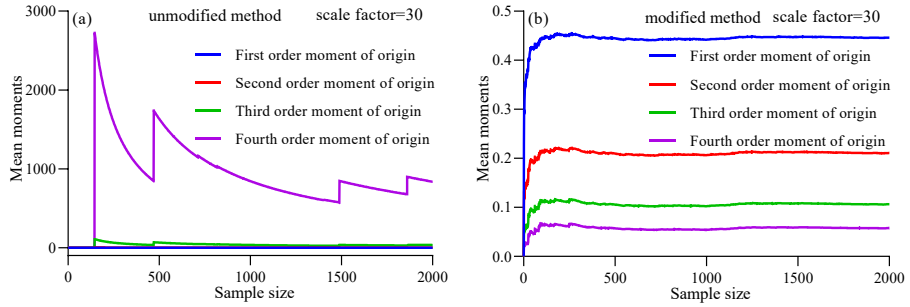

Fig. 12. The mean values of the origin moment of each order: (a) unmodified and (b) modified.

Table 9 The probability of failure of the cut-off point.

Modified MEP	
The cut-off point k /m	Probability of failure
0.8	2.22%
0.9	3.37%
1.0	3.82%
1.1	3.77%
1.2	3.77%
1.3	3.77%
1.4	2.94%
1.5	2.62%

Table 10 Probability of failure and relative errors of the two methods (scale factor = 30).

	QMC	Modified MEP
Probability of failure	3.92%	3.82%
Relative error	2.55%	

Table 11 Probability of failure and relative errors of the methods (scale factor = 29).

	QMC	Modified MEP

Probability of failure	2.12%	2.19%
Relative error	3.30%	

Table 12 Probability of failure and relative errors of the methods (scale factor = 28).

	QMC	Modified MEP
Probability of failure	1.12%	1.06%
Relative error	5.36%	

5.4 Bounds of the IDA curves of the structures with uncertainties

In the sampling, when the parameters such as the maximum structural internal load, the minimum elasticity modulus, the minimum damping ratio, and the minimum yielding strength in a structure with uncertainties are drawn at the same time, this is the most dangerous situation for the structure stability, and it is determined to be the unfavourable case in this paper. Similarly, according to the analysis, the most favourable case can also be defined. It should be noted that for the deviations of the nodes, it is difficult to determine the most dangerous effects because of the randomness of their spatial locations; therefore, in this case, the node deviations are not considered. Thus, the unfavourable bound of the IDA curve under the earthquake Big Bear-01 can be approximately estimated, as shown in **Fig. 13**.

From **Fig. 13**, it can be seen that when the structure loses stability, the PGAs of the two cases are 17.11 m/s^2 and 37.22 m/s^2, respectively. This means that when the PGA is larger than 37.22 m/s^2, whether it is a perfect structure or a structure with uncertainties, the structure will certainly lose stability. When the PGA is less than 17.11 m/s^2, the probability of structural failure is extremely low, which depends on the randomness of the node errors, and the uncertainty of the parameter increases the probability of structural failure.

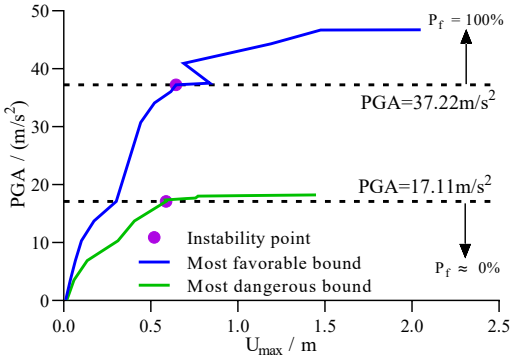

Fig. 13. IDA curves of the unfavourable and favourable cases.

6. Discussion

Compared with the conventional methods, the used, improved, and proposed methods in this paper are substantial, and the results for the instability and the failure probability analyses have high reliability.

Compared with the constant step algorithm, the interpolation algorithm used in this paper can capture the instability points more accurately and steadily. Through improving the statistical parameters in the small sample using the bootstrap calibration method, the calculated probability of failure in the seismic fragility analysis has a higher precision.

Compared with the direct MC sampling method, computing the probability of structural failure requires less time based on the QMC. The use of the improved MEP method can further reduce the calculation time of the probability of structural failure and solve the divergence problem in the conventional MEP method. The relative estimation error for the probability of structural failure is approximately 5%.

With the wide use of parallel computing,[13] it is natural to utilize this promising method to speed up IDA calculations. However, there are some limitations to the current study. For the IDA interpolation algorithm in this paper, it is difficult to use the multicore parallel computing for an IDA curve because the follow-up calculation needs the result from the previous step. In addition, in **Fig. 15**, the node deviations are difficult to consider. Therefore, the estimation of the PGA in the unfavourable case is an approximation.

7. Conclusions

In the present study, the IDA instability algorithm, the modified seismic fragility analysis based on the bootstrap calibration method, and the collapse probability of dynamic instability using the QMC and MEP methods are investigated for the single-layer latticed dome. According to the above results, the following conclusions can be drawn:

- The vertical displacement ratio (VDR) is quantified, which is within the range of 0.5 and 1, and the single-layer latticed dome is a vertical-displacement-sensitive structure.
- $U_{max,-Z}$ can directly replace $|U'_Z|$ or U_{max} to simplify the calculation and can be used to investigate the problems of the structural instability. The instability of the structure first comes from the nodes that are close to the supports.
- The structural design parameters, such as the load and span-depth ratio, have a small effect on U_{max} when the PGAs are small, but when the PGAs are large, the effect increases. Through the IDA for the unfavourable case, the PGA of the earthquake ground motion resulting in structural instability with an extremely low failure probability can be approximately estimated.

Acknowledgements

The financial support from the National Key Research and Development Program of China (Grant No. 2018YFC1504304), the National Natural Science Foundation of China (Grant No. 51878433), and the Key Project of the Natural Science Foundation of Tianjin City (Grant No. 19JCZDJC39300) is acknowledged.

References

1. Zhang HD and Han QH, A numerical investigation of seismic performance of large span single-layer latticed domes with semi-rigid joints, *Struct Eng Mech.* **48**(1) (2013) 57-75. https://doi.org/10.12989/sem.2013.48.1.057.
2. Bradley BA, A critical examination of seismic response uncertainty analysis in earthquake engineering, *Earthquake Engineering and Structural Dynamics* **42**(11) (2013) 1717-1729. https://doi.org/10.1002/eqe.2331.
3. Hess P, Bruchman D, Assakkaf I and Ayyub B, Uncertainties in Material and Geometric Strength and Load Variables, *Naval Engineers Journal.* **114** (2002) 139-166. https://doi.org/10.1111/j.1559-3584.2002.tb00128.x.
4. Kareem A and Gurley K, Damping in structures: its evaluation and treatment of uncertainty, *Journal of Wind Engineering and Industrial Aerodynamics.* **59**(2) (1996) 131-157. https://doi.org/https://doi.org/10.1016/0167-6105(96)00004-9.
5. Mang H, Schranz C and Mackenzie-Helnwein P, Conversion from imperfection-sensitive into imperfection-insensitive elastic structures I: Theory, *Computer Methods in Applied Mechanics and Engineering.* **195** (2006) 1422-1457. https://doi.org/10.1016/j.cma.2005.05.024.

6. Mousavi MA, Abedi K and Chenaghlou M, Imperfection Sensitivity Analysis of Double Domes Free Form Space Structures, *International Journal of Structural Stability and Dynamics*. **15**(04) (2015) 1450067. https://doi.org/10.1142/s0219455414500679.
7. Vryzidis I, Stefanou G and Papadopoulos V, Stochastic stability analysis of steel tubes with random initial imperfections, *Finite Elements in Analysis and Design*. **77** (2013) 31-39. https://doi.org/https://doi.org/10.1016/j.finel.2013.09.002.
8. Chen G, Zhang H, Rasmussen KJR and Fan F, Modelling geometric imperfections of spatial latticed structures considering correlations of node imperfections, *Applied Mechanics and Materials*. **553** (2014) 576-581. https://doi.org/10.4028/www.scientific.net/AMM.553.576.
9. Zhong J, Zhi XD and Fan F, Sensitivity of Seismic Response and Fragility to Parameter Uncertainty of Single-Layer Reticulated Domes, *Int J Steel Struct*. **18**(5) (2018) 1607-1616. https://doi.org/10.1007/s13296-018-0057-3.
10. Zhang HD, Zhu XQ and Yao S, Nonlinear dynamic analysis method for large-scale single-layer lattice domes with uncertain-but-bounded parameters, *Engineering Structures*. **203** (2020) 109780. https://doi.org/10.1016/j.engstruct.2019.109780.
11. Kayhani H, Azarbakht A and Ghafory-Ashtiany M, Estimating the annual probability of failure using improved progressive incremental dynamic analysis of structural systems, *Struct Des Tall Spec Build*. **22**(17) (2013) 1279-1295. https://doi.org/10.1002/tal.1006.
12. Liang H, Guo S, Tu J and Li D, Seismic Stability Sensitivity and Uncertainty Analysis of a High Arch Dam-Foundation System, *International Journal of Structural Stability and Dynamics*. **19**(07) (2019) 1950066. https://doi.org/10.1142/s0219455419500664.
13. Vamvatsikos D, Performing incremental dynamic analysis in parallel, *Computers & Structures*. **89** (2011) 170-180. https://doi.org/10.1016/j.compstruc.2010.08.014.
14. Yang DB, Yun CG, Wu JZ and Yao YL, Seismic response and failure mechanism of single-layer latticed domes with steel columns and braces as substructures, *Thin-Walled Structures*. **124** (2018) 458-467. https://doi.org/10.1016/j.tws.2017.12.038.
15. Hariri-Ardebili MA and Saouma VE, Collapse Fragility Curves for Concrete Dams: Comprehensive Study, *Journal of Structural Engineering (ASCE)*. **142**(10) (2016) 1-13. https://doi.org/10.1061/(ASCE)ST.1943-541X.0001541.
16. Jiongo VD and Nguimkeu P, Bootstrapping mean-squared errors of robust small-area estimators: Application to the method-of-payments surveys data, *Scand J Stat*. **46**(4) (2019) 1274-1299. https://doi.org/10.1111/sjos.12394.
17. Wang YQ, Zhou WH, Dong DF and Wang ZY, Estimation of random vibration signals with small samples using bootstrap maximum entropy method, *Measurement*. **105** (2017) 45-55. https://doi.org/10.1016/j.measurement.2017.04.003.
18. Shun-Fang W, Fu-Lai K and Huai-Xiong Z, Improved PCA facial recognition with bootstrap and data standardization in small sample case, in *Proceedings of 2011 International Conference on Computer Science and Network Technology* (2011). https://doi.org/10.1109/ICCSNT.2011.6182504.
19. Bertsimas D and Sturt B, Computation of Exact Bootstrap Confidence Intervals: Complexity and Deterministic Algorithms, *Oper Res*. **68**(3) (2020) 949-964. https://doi.org/10.1287/opre.2019.1904.
20. Hou TF, Nuyens D, Roels S and Janssen H, Quasi-Monte Carlo based uncertainty analysis: Sampling efficiency and error estimation in engineering applications, *Reliab Eng Syst Saf*. **191**

(2019) 14. https://doi.org/10.1016/j.ress.2019.106549.
21. Dick J, Kuo FY and Sloan IH, High-dimensional integration: The quasi-Monte Carlo way, *Acta Numer.* **22** (2013) 133-288. https://doi.org/10.1017/s0962492913000044.
22. Hou Y, Wang X and Guo J, Quasi Monte Carlo method for reliability evaluation of power system based on Dimension Importance Sorting, *International Transactions on Electrical Energy Systems.* **27**(3) (2017) 1-14. https://doi.org/10.1002/etep.2264.
23. Kucherenko S, Albrecht D and Saltelli A, Exploring multi-dimensional spaces: a Comparison of Latin Hypercube and Quasi Monte Carlo Sampling Techniques, (2015). https://arxiv.org/abs/1505.02350
24. Deng Y, Ding YL, Li AQ and Zhou GD, Prediction of extreme wind velocity at the site of the Runyang Suspension Bridge, *Journal of Zhejiang University: Science A.* **12**(8) (2011) 605-615. https://doi.org/10.1631/jzus.A1000446.
25. He X and Lu Z, Seismic fragility assessment of a super tall building with hybrid control strategy using IDA method, *Soil Dynamics and Earthquake Engineering.* **123** (2019) 278-291. https://doi.org/10.1016/j.soildyn.2019.05.003.
26. Zhang HD and Wang YF, Energy-based numerical evaluation for seismic performance of a high-rise steel building, *Steel and Composite Structures.* **13**(6) (2012) 501-519. https://doi.org/10.12989/SCS.2012.13.6.501.
27. Hamburger R, Hooper J, Sabol T, Shaw R, Reaveley L, Tide R, Hall W, Barsom J, Ferch R, Galambos T, Gross J and Harris J, Recommended Seismic Evaluation and Upgrade Criteria for Existing Welded Steel Moment-Frame Buildings, (2000). https://doi.org/http://gen.lib.rus.ec/book/index.php?md5=cc2760865ad9a433c7ffea05d25671b1.
28. Vamvatsikos D and Allin Cornell C, Incremental dynamic analysis, *Earthquake Engineering and Structural Dynamics.* **31**(3) (2002) 491-514. https://doi.org/10.1002/eqe.141.
29. Zhong J, Zhang J, Zhi X and Fan F, Probabilistic seismic demand and capacity models and fragility curves for reticulated structures under far-field ground motions, *Thin-Walled Structures.* **137** (2019) 436-447. https://doi.org/10.1016/j.tws.2019.01.032.
30. Yu Z, Lu C, Ma H and Kong F, Probabilistic seismic vulnerability assessment of aluminium alloy reticulated shells with consideration of uncertainty, *Engineering Structures.* **195** (2019) 288-298. https://doi.org/10.1016/j.engstruct.2019.05.093.
31. Hesterberg TC, What Teachers Should Know About the Bootstrap: Resampling in the Undergraduate Statistics Curriculum, *American Statistician.* **69**(4) (2015) 371-386. https://doi.org/10.1080/00031305.2015.1089789.
32. Ecuyer PL, Quasi-Monte Carlo methods in finance, in *Proceedings of the 2004 Winter Simulation Conference, 2004* (2004). https://doi.org/10.1109/WSC.2004.1371512.
33. Bratley P and Fox BL, Algorithm 659: Implementing Sobol's Quasirandom Sequence Generator, *ACM Transactions on Mathematical Software (TOMS).* **14**(1) (1988) 88-100. https://doi.org/10.1145/42288.214372.
34. Wan HP and Ren WX, Parameter selection in finite-element-model updating by global sensitivity analysis using gaussian process metamodel, *Journal of Structural Engineering (ASCE).* **141**(6) (2015) 1-11. https://doi.org/10.1061/(ASCE)ST.1943-541X.0001108.
35. Rockinger M and Jondeau E, Entropy densities with an application to autoregressive conditional skewness and kurtosis, *Journal of Econometrics.* **106**(1) (2002) 119-142.

https://doi.org/10.1016/S0304-4076(01)00092-6.
36. Goulet C, Haselton B, Mitrani-Reiser J, Beck J, Deierlein G, Porter K and Stewart J, Evaluation of the seismic performance of a code-conforming reinforced-concrete frame building - From seismic hazard to collapse safety and economic losses, *Earthquake Engineering & Structural Dynamics*. **36** (2007) 1973-1997. https://doi.org/10.1002/eqe.694.
37. Haselton C, Goulet C, Mitrani-Reiser J, Beck J, Deierlein G, Porter K, Stewart J and Taciroglu E, An Assessment to Benchmark the Seismic Performance of a Code-Conforming Reinforced-Concrete Moment-Frame Building, (2008). https://peer.berkeley.edu/sites/default/files/web_peer712_curt_b._haselton_christine_a._goulet_judith_mitrani-reiser.pdf
38. Dolsek M, Incremental dynamic analysis with consideration of modeling uncertainties, *Earthquake Engineering & Structural Dynamics*. **38** (2009) 805-825. https://doi.org/10.1002/eqe.869.
39. Melchers RE and Beck AT, Resistance Modelling, Structural Reliability Analysis and Prediction, (2018) 273-292. https://doi.org/10.1002/9781119266105.ch8.
40. Gan T, Delin L, Caiqi Z and Huilin Z, Statistical Regulation and Parameter Study on Initial Geometrical Imperfections of Spatial Structures Based on Measured Data, *Building Structure.* (02) (2008) 74-78. https://doi.org/10.19701/j.jzjg.2008.02.022.
41. Cai J, He S, Jiang Z, Zhang Y and Liu Q, Investigation on maximum value of initial geometric imperfection in stability analysis of single layer reticulated shells, *Jianzhu Jiegou Xuebao/Journal of Building Structures.* **36**(6) (2015) 86-92. https://doi.org/10.14006/j.jzjgxb.2015.06.011.
42. Zhang HD, Wang JP, Zhang XS and Liu GP, Effects of viscous damping models on a single-layer latticed dome during earthquakes, *Struct Eng Mech.* **62**(4) (2017) 455-464. https://doi.org/10.12989/sem.2017.62.4.455.
43. Zhang H, Wang Y and Han Q, Nonlinear material loss factors of single-layer latticed domes subjected to earthquake ground motions, *Journal of Structural Engineering (ASCE).* **141**(7) (2015). https://doi.org/10.1061/(ASCE)ST.1943-541X.0001149.
44. Moghaddam HA, Seismic behaviour of space structures, *International Journal of Space Structures.* **15**(2) (2000) 119-135. https://doi.org/10.1260/0266351001495026.